Magnetic Forces And Magnetized Biomaterials Provide Dynamic Flux Information During Bone Regeneration

Magnetic Forces And Magnetized Biomaterials Provide Dynamic Flux Information During Bone Regeneration

Alessandro Russo [a], Michele Bianchi [a], Maria Sartori [c], Annapaola Parrilli [c], Silvia Panseri [d], Alessandro Ortolani [b], Monica Sandri [d], Marco Boi [a], Donald M Salter [e], Maria Cristina Maltarello [f], Gianluca Giavaresi [c,g], Milena Fini [c,g], Valentin Dediu [h], Anna Tampieri [d], Maurilio Marcacci [a,b].

[a] Laboratorio di NanoBiotechnologie (NABI), Istituto Ortopedico Rizzoli, via di Barbiano 1/10, 40136 Bologna, Italy.

[b] Laboratorio di Biomeccanica ed Innovazione Tecnologica, Istituto Ortopedico Rizzoli, via di Barbiano 1/10, 40136 Bologna, Italy.

[c] Laboratorio di Biocompatibilità Innovazioni Tecnologiche e Terapie Avanzate (BITTA), Istituto Ortopedico Rizzoli, via di Barbiano 1/10, 40136 Bologna, Italy.

[d] Istituto di Scienza e Tecnologia dei Materiali Ceramici (ISTEC), Consiglio Nazionale delle Ricerche, via Granarolo 64, 48018 Faenza, Italy.

[e] Institute of Genetics and Molecular Medicine, University of Edinburgh, EH4 2XU Edinburgh, United Kingdom,

[f] Laboratorio di Biologia cellulare muscoloscheletrica, Istituto Ortopedico Rizzoli, via di Barbiano 1/10, 40136 Bologna, Italy.

[g] Laboratorio Studi Preclinici e Chirurgici, Istituto Ortopedico Rizzoli, via di Barbiano 1/10, 40136 Bologna, Italy.

[h] Istituto per lo Studio dei Materiali Nanostrutturati (ISMN), Consiglio Nazionale delle Ricerche, , via Gobetti 101, 40129 Bologna, Italy.

Corresponding author: Alessandro Russo

Laboratorio di NanoBiotechnologie (NABI)

Istituto Ortopedico Rizzoli

Via Gobetti 1/10, 40136 Bologna, Italy

T: +39-0516366983

F: +39-051583789

E: a.russo@biomec.ior.it

Abstract

The fascinating prospect to direct tissue regeneration by magnetic activation has been recently explored. In this study we investigate the possibility to boost bone regeneration in an experimental defect in rabbit femoral condyle by combining static magnetic fields and magnetic biomaterials. NdFeB permanent magnets are implanted close to biomimetic collagen/hydroxyapatite resorbable scaffolds magnetized according to two different protocols. Permanent magnet only or non-magnetic scaffolds are used as controls. Bone tissue regeneration is evaluated at twelve weeks from surgery from a histological, histomorphometric and biomechanical point of view. The reorganization of the magnetized collagen fibers under the effect of the static magnetic field generated by the permanent magnet produces a highly-peculiar bone pattern, with highly-interconnected trabeculae orthogonally oriented with respect to the magnetic field lines. In contrast, only partial defect healing is achieved within the control groups. We ascribe the peculiar bone regeneration to the transfer of micro-environmental information, mediated by collagen fibrils magnetized by magnetic nanoparticles, under the effect of the static magnetic field. These results open new perspectives on the possibility to improve implant fixation and control the morphology and maturity of regenerated bone providing "in site" forces by synergically combining static magnetic fields and biomaterials.

1. Introduction

Throughout life bone is continuously subjected to a range of mechanical forces that influence both its external geometry and internal architecture.[1] Adaptation of bone to the mechanical environment is due to targeted activation of bone multicellular units with pre-existing bone being initially removed by osteoclasts and subsequently replaced by osteoblastic activity.[2] The remodelling process is known to be a low energy process governed by both genetic and environmental information.[3,4] Environmental cues, such as mechanical loads, determine extracellular matrix (ECM) allosteric variation and cellular arrangement of bone in order to optimize biomechanical function.[5] At the lowest hierarchical level in the structure of the bone ECM is tropocollagen. Tropocollagen comprises three polypeptide molecules that are folded in the characteristic triple helical configuration to produce a rod-like molecule with a length of about 300 nm and a diameter of around 1.5 nm.[6] The inorganic component of bone comprises hydroxyapatite (HA) crystals 25-50 nm in size, densely deposited onto the collagen fibrils.[7] At the beginning of the mineralization process apatite crystals nucleate from an amorphous phase in the less dense zone of the collagen fibril and subsequently grow in the c-axial length following the long axis of the collagen.[8,9] The

stereochemical interaction of collagen fibers with HA crystals determines the 3D architecture of bone and its material properties.

A major problem in orthopedics is how to best treat patients with a critical sized bone defect. Bone can spontaneously heal when the degree of bone loss is smaller than a critical size that depends on a variety of factors including bone type, segment and animal species.[10] Above the critical size a bone defect will not heal without intervention. Living systems such as cells and tissues can be described as stable but far from thermodynamic equilibrium systems with input energy used to enforce stability or repair damage.[11,12] Such a system can maintain order over long periods of time but only in the absence of significant perturbations. If the energy in-flow stops the system order declines rapidly to equilibrium and death.[13] From a thermodynamic point of view the failure to repair a critical bone defect may be explained by a loss of information from the environment with an increase in the level of entropy until equilibrium is reached, biologically equating to formation of fibrous scar tissue rather than highly organized bone.[13]

A number of tissue engineering approaches have been developed during the last decades aiming to repair critical sized bone defects. These have been focused predominantly on bone autografts, allografts or synthetic graft material in addition to the use of novel scaffolds mainly based on calcium phosphates and hydroxyapatite.[14-17] Other methodologies such as the combined use of static magnetic fields and magnetic nanoparticles, whose effects on bone cell proliferation and differentiation have recently been investigated, are of increasing interest.[18] In particular, magnetic nanoparticles have been extensively investigated as suitable vectors for applying forces to and mechanically conditioning single cells or populations of cells.[19,20] Application of a strong static magnetic field to the system induces a high magnetic gradient field that causes displacement of the particles along the gradient vector with the production of compression and tensile forces on the cell membrane resulting in cytoskeleton deformation and cell dragging.[21] Mechanical forces, transmitted to the cytoskeleton by membrane receptors such as integrins, are envisaged to activate a number of intracellular signaling pathways including changes in intracellular calcium levels and MAP kinase activity that replicate the effect of mechanical loading and regulate osteocyte and osteoblast function eventually leading to the development and normal function of bone tissue.[22-28] Recently we proposed a novel approach to stimulation of bone growth by exploiting the synergic effect of static magnetic fields and magnetized biomimetic materials.[29-31] Initial studies demonstrated that a biomimetic and biodegradable scaffold magnetized with magnetic iron oxide nanoparticles implanted in contact with a titanium coated permanent magnet in an experimental bone defect in a rabbit condyle was able to dynamically re-organize its internal structure over a four week follow-up period, strongly influencing newly-formed bone tissue volume.[32]

In the current study we present the pattern of bone regeneration after twelve weeks of follow-up in an experimental bone defect model in rabbit femoral condyle treated by a hybrid biomimetic collagen/HA scaffold magnetized with magnetic nanoparticles according to two different protocols and implanted close to a titanium-coated permanent magnet. We show that the synergic combination of magnetic forces and magnetized biomaterials is able to generate a characteristic bone pattern with dense and highly-interconnected bone trabeculae orthogonally oriented nearly with respect to the magnetized collagen fibrils and parallel to the isomagnetic lines of the permanent magnet.

2. Methods

2.1 Synthesis of the Magnetic Scaffolds

Four different groups (two magnetic groups and two control groups) were considered in this study (**Figure 1, top**).

Collagen/HA hybrid magnetic scaffolds were prepared following two different protocols. Method A is based on the concurrent nucleation of biomimetic hydroxyapatite and 7 wt. % ferromagnetic nanoparticles (MNPs, Aldrich n.637106, iron (II, III) oxide, < 50 nm uncoated particles; Sigma-Aldrich, St. Louis, MO, USA) on self-assembling type I collagen fibrils, thus realizing the magnetization of the scaffold material *in situ* (Magnetic scaffold A: MAG-A).[33] The mineralization process was performed following an acid-base neutralization process in the presence of the ferromagnetic nanoparticles. The process induces the formation of the hydroxyapatite nano-nuclei in direct contact with the collagen matrix and the simultaneous entrapment of the magnetic nanoparticles in the collagen fibres. The dried cylindrical porous samples were finally obtained by a controlled freeze-drying process (Magnetic scaffold A: MAG-A).[33] Method B is based on the infiltration of collagen/HA hybrid porous scaffolds with a ferro-fluid solution leaving ferromagnetic nanoparticles entrapped in the construct. The scaffolds were then freeze-dried after rinsing (Magnetic scaffold B: MAG-B).[34] The ferro-fluid solution referred to as FF-DP is an aqueous dispersion of magnetite nanoparticles coated with starch and functionalized with phosphate groups (density: 2.5 mg ml^{-1}; mean size of the nanoparticles ~ 200 nm; Chemicell GmbH, Berlin, Germany). As a consequence of the adopted synthesis method the scaffolds became magnetic whilst maintaining their specific porosity and shape. All the cylindrical scaffolds, 4-mm in diameter and 4-mm in height, were placed inside single surgical packs and sterilized by γ-ray radiation (25 kGy). Two control groups were selected for this experiment: the first control group (MAG C) consisted of the implantation of the NdFeB magnets alone, thus leaving the experimental defect empty. Cylindrical NdFeB magnets (8.00 mm high x 2.00 mm diameter; 1.2 T) were coated with a titanium capsule (thickness: 200 μm) to increase its biocompatibility (especially due to the formation of a thin layer of titanium oxide on the surface) and to avoid surface corrosion which could result in local

toxicity when implanted in bone tissue. NdFeB magnets were sterilized by γ-ray radiation (25 kGy). The second control group (MAG D) consisted of commercial biomimetic and re-absorbable porous scaffolds, 4-mm in diameter and 2-mm in height, obtained by biologically inspired nucleation of biomimetic hydroxyapatite on self-assembling type I collagen fibres 70/30 wt.%, (RegenOss, Fin-Ceramica SpA, Italy).[35,36] All the scaffolds evidenced a similar porous architecture (porosity ~ 87-89 % for MAG A and MAG D, ~ 89-91 % for MAG B) with a tri-dimensional fibrous network suitable for cell penetration and scaffold vascularization (**Fig. 1, bottom**). Mean pore size was ~ 200-350 μm for all the scaffolds. The saturation magnetization was ~ 15 emu/g for MAG A and ~ 20-23 emu/g for MAG B. [37]

2.2 *In Vivo* Study

The *in vivo* study was performed following European and Italian Law on animal experimentation, after the approval of the research protocol by the Ethical Committee of Rizzoli Orthopaedic Institute and by the responsible public authorities in accordance with EU regulations. Twelve male rabbits (Charles River, Calco, Lecco, Italy), 2.5 ± 0.3 Kg body weight, were housed singularly at a controlled temperature of 22 ± 1°C and relative humidity of 55 ± 5 % and fed a standard diet (Mucedola, Settimo Milanese, Milano, Italy) with filtered tap water *ad libitum*. General anaesthesia was induced by intramuscular injection of 44 mg/kg ketamine (Imalgene 1000, Merial Italia S.p.A, Assago-Milan, Italy) and 3 mg/kg xylazine (Rompun, Bayer SpA, Milano, Italy) under assisted ventilation with O_2/air (1/0.4 $lmin^{-1}$) mixture and 2.5% isofluorane (Forane, Abbot SpA, Campoverde di Aprilia-Latina, Italy). Cylindrical defects (2.0 mm in diameter and 12.0 mm in depth) were created bilaterally in the lateral condyle of the distal femoral epiphysis by using a drill; thereafter the defects were widened up to 4.0 mm in diameter to a depth of 4.0 mm. The defects were flushed with cold sterile 0.9% NaCl solution during the surgical procedure to prevent the risk of bone necrosis. A cylindrical NdFeB magnet was implanted in each defect. Thereafter a magnetic and/or control scaffold was pressed into the defect in order to position the materials as shown in Figure 1a. Postoperatively antibiotics and analgesics were administered: 0.6 ml/kg flumequil (Flumexil, (FATRO SpA. Ozzano Emilia - Bologna- Italy) and 0.1 ml/kg/day metamizole sodium (Farmolisina, Ceva Vetem SpA, Porto Empedocle-Grosseto, Italy). At 12 weeks after surgery animals were euthanized with an intravenous administration of Tanax (Hoechst, Frankfurt am Main, Germany) under general anaesthesia. Femoral condyles were excised, stripped of soft tissue and the presence of haematomas, oedema, and inflammatory tissue reactions was macroscopically evaluated.

2.3 Histologic and Histomorphometric Evaluations

The distal femoral epiphyses were processed for undecalcified bone studies. After fixation in 4% (v/v) buffered paraformaldehyde, samples were dehydrated in a graded series of alcohol/water mixture for 24 hours each (50°, 70° and two passages in 95°), followed by complete dehydration in absolute alcohol. After removal of water from the specimens a 24 h-infiltration period in methyl methacrylate was performed to prepare the tissue for final embedding in poly-methyl methacrylate resin (Merck, Schuchardt, Hohenbrunn, Germany). Embedded bone samples were longitudinally sectioned along a plane parallel to the long axis of the implant with the cutting system EXAKT (EXAKT Apparatus GmbH, Norderstedt, Germany). The cutting plane allowed the simultaneous visualisation of the entire length of the NdFeB magnets and the magnetic and/or control scaffolds as shown in Figure 1b. Histological sections, up to ≈ 10 µm thickness, were stained with Toluidine Blue, Acid Fuchsin and Fast Green for subsequent histomorphometric analysis. For all the histological images reported in the present manuscript, bone tissue appears grey/light blue, the residual scaffold material (magnetized collagen fibers) is brownish, the permanent magnet is black and the bone marrow (infiltrated by PMMA) appears white/transparent. Bone histomorphometry measurements were performed semi-automatically using an optic microscope (BX51, Olympus Optical Co. Europa GmbH, Germany) connected to an image analyser system (Qwin, Leica Imaging Systems Ltd., United Kingdom). Through the image analyser system a defined region of interest (ROI) of 1400 x 1400 pixels was drawn at the interface between NdFeB magnets and magnetic or control scaffold for the middle histological sections. Inside each selected ROI the quantification of new bone formation (Bone Volume/Total volume, BV/TV, %) and residual material area (Material Volume/Total Volume, Mat.V/TV, %) was carried out through an image binarization process in Hue Saturation and Brightness (HSB) color space.

The local orientation of the newly formed bone trabeculae in the defect region was evaluated and quantified using OrientationJ, an ImageJ plug-in in three condyles for each group.[38] For this analysis, a region of interest (ROI) was selected within the defect area, having the same height of the permanent magnet but separated by 500 µm from its surface. This choice was driven by the necessity to exclude the newly-formed bone trabeculae grown on the biocompatible titanium oxide magnet surface, i.e. not influenced by the presence of the magnetic field but significantly biasing the final results of the analysis. In this ROI, bone tissue was digitally isolated from the background and from the residual scaffold material, by binarizing the image through the HSB color space. After that, a Gaussian gradient-based structure tensor was calculated with a Gaussian window of 5 pixels (corresponding to 20 µm and considered as the minimum size of the new single trabecula). Coherency was set at 70% in order to discriminate only the significantly-oriented structures. The orientation of the trabeculae with respect to the central axis of permanent magnet was measured and results reported as different colors according to a scale from - 90°

to + 90°. A ~ 0° value corresponded to bone trabeculae parallel to the magnetic field lines, whereas a value close to ± 90° was related to trabeculae orthogonal to the magnetic field lines. The histograms of the local angular orientations normalized by the overall number of trabeculae were then obtained; finally, the trabecular orientation values falling in the intervals + (-) 90° to + (-) 80° and - 10° to + 10° were statistically analyzed for all the investigated groups.

2.4 Scanning Electron Microscopy (SEM) Analysis

Methyl methacrylate embedded magnetic scaffolds and bone segments were polished using diamond paste and gold sputtered (film thickness ~ 5 nm) before being studied with a Scanning Electron Microscope (SEM, Cambridge Stereoscan200, Cambridge, UK) equipped with a backscattered electron detector (BSE). Bone morphology, magnetized scaffold collagen fibre orientation as well as the presence of iron oxide nanoparticles within new bone tissue, was investigated by Energy dispersive X-ray Spectroscopy: analyses were carried out at 20kV acceleration potential, 25 mm working distance and 100 s of acquisition time with an Oxford INCA Energy 200 apparatus.

2.5 Nanoindentation Analysis

On polished PMMA-embedded histological slides, suitable regions of interest (ROIs) were selected for nanoindentation analysis, both in the area of implantation (newly-formed bone) and far from the area of implantation (native bone). Three condyles for each group have been studied with the number of useful indents for each bone type within each condyle ranging from 57 to 82. The overall number of indents for each group (MAG A, MAG B, MAG C and MAG D) ranged from 126 to 200 depending on the amount of bone available for nanoindentation tests. Bone regions located at the border between mature and native bone or very close to the magnet side, i.e. not clearly ascribable to one specific bone type were excluded from the data set. For each ROI variable-size two-dimensional matrixes of indents were set up; the distance among subsequent indents was 20 microns in both x and y directions to avoid any influence of residual stresses due to adjacent indentations.[39,40] The mapping procedure of reduced elastic modulus (E_R) and contact hardness (H_c) was performed using a nanoindentation tester (NHT^2, CSM Instruments SA, Peseux, Switzerland) equipped with a diamond Berkovic tip. Instrument calibration was performed before nanoindentation tests by measuring indents of increasing depth in fused quartz with an indentation modulus of 72 GPa. E_R and Hc were estimated according to the method by Oliver and Parr (2004).[41,42] In order to limit the viscoelasticity contribution due to the time dependent behavior of bone, a creep hold of 60 s has been introduced at peak load.[39] The following procedure was used for the analyses: a linear loading (loading and unloading rate set at 30 mN/min)

for a maximum load of 10 mN.[43] The control of the thermal drift was automatically performed by the system between each indentation. All the data corresponding to unrealistic low elastic modulus measurements (E < 4GPa, evidently ascribable to indents performed on bone-surrounding PMMA) and to indents performed on or near the edge between bone and PMMA were considered outliers and removed from the dataset. Data corresponding to explicitly inadequate contact points were excluded from the data set. E_r and H_c of newly-formed and native bone were provided as well as the mechanical gap (%), i.e. the difference between the modulus (and hardness) of the native bone and the modulus (and hardness) of the newly-formed bone.

2.6 Statistical Analysis

Statistical analysis was performed using the MATLAB software (version 7.13.0.564, Mathworks, Natick, MA, USA). After having verified the normal distribution of data, the one-way ANOVA followed by the post hoc Bonferroni test was used to compare histomorphometric, nanoindentation data and trabecular orientation data. Data are reported as mean values ± standard deviation, at a significance level of $p < 0.05$.

3. Results

3.1 Histological and Histomorphometric Analysis

There were no intra- or post-operative complications. At the end of the experiment explanted bone segments and surrounding tissues did not show signs of infection, oedema or peri-implant soft tissue reactions associated with either the magnetic and control scaffolds or to the NdFeB magnet. A total of 24 bone samples in which the scaffolds and NdFeB magnets retained the correct positioning as indicated by the radiological and histological investigations (representative images are shown in **Figure 2a** and **Figure 2b**, respectively) were retrieved at 12 weeks.

There was no histological evidence of an adverse interaction between static magnetic field exposure and bone tissue formation and growth. The NdFeB magnets appeared well osteo-integrated with the surrounding cancellous bone as suggested by the direct apposition of bone onto the surface of the magnet (**Figure 2c**). There was no evidence of a mononuclear histiocyte, multinucleated giant cell, lymphocyte or plasma cell infiltrate or region of interposed fibrous capsule in relation to the magnet (as in the case of not implanted animals, **Figure 2d**). There was neither necrosis nor inflammation in relation to the presence of corrosion products or magnetic nanoparticles.

When analyzing the morphology of the regenerated bone pattern, in the MAG A group the combined effect of magnetic forces and magnetized biomaterials resulted in complete sealing of the experimental defect by a deeply interconnected bone trabeculae net (**Figure 3a**). Collagen fibers from the dissolving scaffold were still coated with magnetite, oriented orthogonally to bone trabeculae (**Figure 3b** and **Figure 4**) and parallel to the magnetic field lines, as a consequence of the magnetic gradient exerted by the static magnetic field on the magnetic nanoparticles bonded to collagen fibers. Both optical (Fig. 3a) and BSE-EDX (**Figure 4a** and **Figure 4b**) images highlighted the presence of mature trabeculae with normal osteocyte lacunae (red stars). Instead, only partial healing of the defect was observed in the MAG B group (**Figure 3c**), where bone trabeculae exhibited a more irregular distribution (Fig. 3d). Contrary to what was observed for the magnetic groups, in both control groups, MAG C (**Figure 3e** and **Figure 3f**) and MAG D (**Figure 3g** and **Figure 3h**), a significant lack of bone tissue was observed in the area of the experimental defect proximal to the magnet.

Despite the considerable differences in term of tissue morphology between the different groups, histomorphometric data revealed no significant differences between the bone volume (BV/TV %) of MAG A and the volume of the control scaffolds (**Figure 5**). Only BV/TV % of MAG B was lower ($p=0.032$) than BV/TV % of MAG C. Concerning Mat.V/TV, MAG A and MAG B were similar ($p= 0.973$). No data for Mat.V/TV were available for MAG C or MAG D due to the absence of the scaffold in the MAG C group and to the fact that the commercial scaffold of MAG D was completely resorbed at 12 weeks after implantation. The results of the analysis of the trabecular orientation have been reported in **Figure 6**. The percentage of oriented trabecular structures in the intervals between + (-) 90° to + (-) 80° was statistically different ($p<0.05$) when comparing MAG A with MAG B or MAG D. The same differences were detected for MAG C versus MAG B and MAG D. Besides, trabeculae in MAG A were less orientated in the -10° to +10° range than trabeculae in the other group, even if this difference was not statistically significant ($p = 0.22$).

The BSE-EDX analysis performed on newly-formed bone trabeculae in order to determine the presence of iron nanoparticles within new bone tissue revealed that, whilst it was possible to identify iron nanoparticles in the less mineralized bone tissue, the more mineralized bone was almost free of iron (**Figure 7**), suggesting that the previous incorporation was subsequently followed by loss of iron nanoparticles from the forming bone tissue.

3.2 Evaluation of the Mechanical Properties of Bone Tissue

The reduced elastic modulus (Er) was higher ($p < 0.05$) for native bone than for new bone (**Table 1**) suggesting a still active regeneration process 12 weeks from implantation.[40] With respect to hardness, only in the MAG A group was Hc similar ($p = 0.52$) between newly-formed bone and native bone. The comparison of mechanical gap data indicated that scaffolds magnetized as in MAG A provided new bone tissue with a higher level of maturation (E gap ~ 6.1%; H gap ~ -2.2%) when compared to either MAG B (E gap ~ 13.9%; H gap ~ 14.5%) and the non-magnetic groups (E gap ~ 19.2%; H gap ~ 15.4% for MAG C and E gap ~ 15.0%; H gap ~ 23.6% for MAG D).

4. Discussion

In this study we investigated for the first time the possibility of boosting bone tissue regeneration in an experimental femur bone defect model by combining static magnetic forces and biomimetic magnetic resorbable scaffolds. At 12 weeks from surgery, a dense and ordered trabeculae framework (**Figure 8b** and **Figure 8d**), orthogonally oriented with respect to the magnetic field lines was obtained. The bone regeneration seen in the presence of both magnetic scaffold and permanent magnet was superior to that seen when a non-magnetic scaffold was implanted (**Figure 8f**). Indeed, despite similar BV/TV % values, healing of the defect was inadequate in the non-magnetic groups as evinced by the evident lack of bone tissue in the regeneration area proximal to the permanent magnet. The results of this study also showed that the magnetization method A (MAG A, MPNs nucleation directly on the collagen fiber during collagen/HA scaffold synthesis) was more efficient when compared to method B (MAG B, scaffold impregnated with a ferro-fluid solution) for inducing bone regeneration and to the two control groups (MAG C, only the magnet; MAG D, magnet and non-magnetic scaffold).

Further, nanoindentation analysis indicated that the mechanical properties of newly-formed bone were closer to the mechanical properties of native of bone in MAG A group when compared to the other groups. It is known that bone maturation can be conveniently assessed through mechanical measurements as the mechanical properties are correlated, to a first approximation, to the degree of mineralization.[44,40] In particular, at 12 weeks from surgery, new bone tissue already achieved the same hardness values of native bone in MAG A, thus the regeneration process could be considered successfully concluded. This did not happen for the ferrofluid-infiltrated magnetic scaffold and for the two control groups, where the mechanical properties of the new bone tissue were still far away from those of the native bone. Therefore, besides the better bone trabeculae architecture, MAG A provided also more mature bone trabeculae than the other groups.

As when only the static magnetic forces (alone or coupled to a non-magnetic scaffold) were present no boosting effect occurred, it appears reasonable to ascribe the peculiar bone trabecular pattern of MAG A to a synergistic effect between static magnetic forces and the biomimetic magnetic scaffold fibers.

It is well known that a number of macromolecules such as collagen and fibrin can be oriented orthogonally to magnetic field lines generated by several tesla permanent magnets.[45,46] Kotani et al. observed alignment of non-magnetic collagen fibers orthogonally magnetic fields under static magnetic fields both *in vitro* and *in vivo*.[47,18] However, the effect of combination of a static magnetic field and magnetic scaffolds on bone regeneration has not been previously addressed. In an earlier study we tested the effect of magnetic scaffolds in the absence of a permanent magnetic field.[31] We observed bone regeneration characterized by woven bone trabeculae completely lacking a regular arrangement. We hypothesized that the random disposition of bone trabeculae in the absence of a permanent magnetic field is due to the random orientation of the nanoparticles spin, leading to an overall null magnetic gradient acting in the regeneration site. Therefore, in the absence of a permanent magnetic field, MNPs did not provide additional functional energy to the system. On the contrary the presence of iron oxide MNPs was rather detrimental for the regeneration process as enhanced bone regeneration was found in the control group (scaffold without MNPs). Subsequently we tested the same biomaterials implanted close to a permanent magnet at four weeks follow-up.[32] For the first time *in vivo* we observed a clear reorganization of the scaffold architecture under the static magnetic field. Magnetized collagen fibers aligned in the same direction of the magnetic field lines generated by the permanent magnet. Bone regeneration occurred in both scaffolds but the bone trabeculae formed did not show any specific geometric pattern and MNPs were dispersed into the new bone tissue.

The rationale for the particular bone growth found in the present study, may be found by observing that cells at the same distance from the permanent magnet lie on the same level of magnetic potential (isomagnetics lines) i.e. they experience the same magnetic force and consequently analogous mechanical stresses. It appears reasonable to postulate that similar mechano-transduction processes may have occurred, activated by the presence of the MNPs, eventually leading to coherent matrix apposition and bone tissue growth in a pattern orthogonal to the magnetic field lines. The observation that a smaller number of structures were exactly oriented at ± 90° in the MAG A group when compared to the MAG C group can be ascribed to steric hindrance due to the presence of the scaffold in the MAG A group. Indeed, newly-formed trabeculae tended to orient orthogonally to the magnetic field lines, as demonstrated by the quantitative analysis in the + (-) 90° to + (-) 80° range, but they had no the same amount of free volume available for bone growth, as for MAG C. However, it should be remarked that this difference was not statistically significant and that MAG C, even if providing similar BV/TV % values, failed to

completely seal the defect. Further, when comparing systems with similar steric hindrance (MAG A, MAG B and MAG D), the synergic positive effect between the permanent magnet and the scaffold was evident in the higher orientation of trabeculae in MAG A compared to MAG B and MAG D.

Magnetic nanoparticles, in turn activated by the static magnetic forces, act as a route by which magnetic information is transferred to the cells. Notably, the ferromagnetic properties of MNPs confer to the biomaterial the possibility of being activated by an external magnetic field and determine a progressive ordered distribution of MNPs along the magnetic lines according to a process referred to as "nano-magnetic actuation".[48] The magnetic information carried and transferred by MNPs is not static but dynamic. Indeed the flux of information continuously changes as magnetic nanoparticles or clusters are attracted toward the permanent magnet by the effect of the magnetic forces. This general and progressive migration of MNPs and magnetized collagen fibers towards the surface of the permanent magnet represents a natural way to reduce the magnetic gradient, with the overall effect of producing a dynamic flux of information. The dynamic nature of this cooperative process is also suggested by the presence of magnetic nanoparticles within less mature bone and their almost total absence in the more mature new bone tissue as revealed by EDX analysis. This observation may indicate an active participation of MNPs in the formation of bone tissue; besides, the absence of MNPs in the more mature bone tissue may indicate that bone remodeling has resulted in removal of the iron oxide nanoparticles which begin to migrate through the three-dimensional bone architecture under the static magnetic forces to accumulate at the surface of the permanent magnet.

Conclusions

The results of this study indicate that the use of a magnetic scaffold in conjunction with a permanent magnet may represent a suitable route to boost bone tissue regeneration. This appears to occur through a multi-stage process, based on the mutual interaction of static magnetic fields, MNPs and possibly bone cell mechanoreceptors, the exact mechanism of which will require further detailed studies for elucidation.

Acknowledgments

This study was partially supported by the European Project "Magnetic Scaffolds for *in vivo* Tissue Engineering" (NMP3-LA-2008-214686).

References

1. Frost HM. Wolff's Law and bone's structural adaptations to mechanical usage: an overview for clinicians. Angle Orthod 1994;64:175-88.
2. LaMothe JM, Hamilton NH, Zernicke RF. Strain rate influences periosteal adaptation in mature bone Med Eng Phys 2005;27:277-84.
3. Robling AG, Turner CH. Mechanical Signaling for Bone Modeling and Remodeling Crit Rev Eukaryot Gene Expr 2009;19:319-38.
4. Peterson LF, Kelly PJ, Janes JM. Ultrastructure of bone: technic of microangiography as applied to the study of bone. Proc Staff Meet Mayo Clin 1957;32:681-6.
5. Ingber DE. Mechanobiology and diseases of mechanotransduction. Ann Med 2003;35;564-77.
6. Fratzl P, Gupta HS, Paschalis EP, Roschger P. Structure and mechanical quality of the collagen–mineral nano-composite in bone. J Mater Chem 2004;14:2115-23.
7. Hassenkam T, Fantner GE, Cutroni JA, Weaver JC, Morse DE et al. High-resolution AFM imaging of intact and fractured trabecular bone. Bone 2004;35:4-10.
8. Nudelman F, Pieterse K, George A, Bomans PH, Friedrich H, Brylka LJ et al. The role of collagen in bone apatite formation in the presence of hydroxyapatite nucleation inhibitors. Nat Mater 2010;9:1004-9.
9. Olszta MJ, Chenga X, Jeea SS, Kumara R, Kima Y, Kaufmane MJ et al. Bone structure and formation: A new perspective. Mater Sci Eng R 2007;58:77-116.
10. Petite H, Viateau V, Bensaïd W, Meunier A, de Pollak C, Bourguignon M et al. Tissue-engineered bone regeneration. Nat Biotechnol 2000;18:959-63.
11. Michel D. Life is a self-organizing machine driven by the informational cycle of Brillouin. Orig Life Evol Biosph 2013;43:137-50.
12. Nicolis G, Prigogine I. Symmetry breaking and pattern selection in far-from-equilibrium systems. Proc Natl Acad Sci USA 1981;78:659-63.
13. Kleidon A, Lorenz RD. Non-equilibrium thermodynamics and the production of entropy: life, earth, and beyond. Springer-Verlag Berlin Heidelberg New York; 2005.
14. Khan Y, Yaszemski MJ, Mikos AG, Laurencin CT. Tissue engineering of bone: Material and matrix considerations J Bone Joint Surg Am 2008;90A:36-42.

15. Garg T, Singh O, Arora S, Murthy R. Scaffold: a novel carrier for cell and drug delivery. Crit Rev Ther Drug Carrier Syst 2012;29:1-63.
16. M. Keeney, J. J. van den Beucken, P. M. van der Kraan, J. A. Jansen. The ability of a collagen/calcium phosphate scaffold to act as its own vector for gene delivery and to promote bone formation via transfection with VEGF(165). Biomater 2010;31:2893-2902.
17. Bianchi M, Urquia Edreira ER, Wolke JG, Birgani ZT, Habibovic P, Jansen JA et al. Substrate geometry directs the in vitro mineralization of calcium phosphate ceramics. Acta Biomater. 2014;10:661-9.
18. Kotani H, Kawaguchi H, Shimoaka T, Iwasaka M, Ueno S, Ozawa H et al. Strong static magnetic field stimulates bone formation to a definite orientation in vitro and in vivo. J Bone Miner Res 2002;17:1814-21.
19. Alenghat FJ, Fabry JB, Tsai KY, Goldmann WH, Ingber DE. Analysis of cell mechanics in single vinculin-deficient cells using a magnetic tweezer. Biochem Biophys Res Commun 2000;277:93-9
20. Fabry B, Maksym GN, Hubmayr DR, Butler JP, Fredburg JJ. Implications for heterogeneous bead behaviour on cell mechanical properties measured via magnetic twisting cytometry. J. Magn. Magn. Mater. 1999;194:120-5.
21. Dobson J, Cartmell SH, Keramane A, El Haj AJ. Principle and Design of a novel magnetic force mechanical conditioning bioreactor for tissue engineering, stem cell conditioning, and dynamic in vitro screening. IEEE Trans Nanobiosci 2006;5:173-7.
22. Wang N, Butler JP, Ingber DE. Mechanotransduction across the cell surface and through the cytoskeleton. Science 1993;260:1124-7.
23. Schmidt C, Pommerenke H, Dürr F, Nebe B, Rychly J. Mechanical stressing of integrin receptors induces enhanced tyrosine phosphorylation of cytoskeletally anchored proteins. J Biol Chem 1998;27:5081-5.
24. Pommerenke H, Schmidt C, Dürr F, Nebe B, Lüthen F, Muller P et al. The mode of mechanical integrin stressing controls intracellular signaling in osteoblasts. J Bone Miner Res 2002;17:603-11.
25. Pommerenke H, Schreiber E, Dürr F, Nebe B, Hahnel C, Möller W et al. Stimulation of integrin receptors using a magnetic drag force device induces an intracellular free calcium response. Eur J Cell Biol 1996;70:157-64.
26. Bierbaum S, Holger N. Tyrosine phosphorylation of 40 kDa proteins in osteoblastic cells after mechanical stimulation of β1-integrins. Eur J Cell Biol 1998;77:60-7.
27. Salter DM, Wallace WHB, Robb JE, Caldwell H, Wright MO. Human bone cell hyperpolarisation response to cyclical mechanical strain is mediated by an interleukin-1autocrine/paracrine loop. J Bone Miner Res 2000;15:1746-55.

28. Hughes S, El Haj AJ, Dobson J. Magnetic micro- and nanoparticle mediated activation of mechanosensitive ion channels. Med Eng Phys 2005;27:754-62.
29. Panseri S, Cunha C, D'Alessandro T, Sandri M, Russo A, Giavaresi G et al. Magnetic hydroxyapatite bone substitutes to enhance tissue regeneration: evaluation in vitro using osteoblast-like cells and in vivo in a bone defect. PLoS ONE 2012;7:e38710.
30. Russo A, Shelyakova T, Casino D, Lopomo N, Strazzari A, Ortolani A et al. A new approach to scaffold fixation by magnetic forces: Application to large osteochondral defects. Med Eng Phys 2012;34:1287-93.
31. Panseri S, Russo A, Giavaresi G, Sartori M, Veronesi F, Fini M et al. Innovative magnetic scaffolds for orthopedic tissue engineering. J Biomed Mater Res A 2012;100:2278-86.
32. Panseri S, Russo A, Sartori M, Giavaresi G, Sandri M, Fini M et al. Modifying bone scaffold architecture in vivo with permanent magnets to facilitate fixation of magnetic scaffolds. Bone 2013;56:432-9.
33. Tampieri A, Landi E, Valentini F, Sandri M, D'Alessandro T, Dediu V et al. A conceptually new type of bio-hybrid scaffold for bone regeneration. Nanotech 2011;22:015104.
34. Bock N, Riminucci A, Dionigi C, Russo A, Tampieri A, Landi E et al. A novel route in bone tissue engineering: magnetic biomimetic scaffolds. Acta Biomater 2010;6:786-96.
35. Scaglione S, Giannoni P, Bianchini P, Sandri M, Marotta R, Firpo G, Valbusa U, Tampieri A, Diaspro A, Bianco P, Quarto R. Sci Rep 2012;*2*:274.
36. Tampieri A, Celotti G, Landi E, Sandri M, Roveri N, Falini G. Biologically inspired synthesis of bone-like composite: Self-assembled collagen fibers/hydroxyapatite nanocrystals. J Biomed Mater Res A 2003;67A:618-625.
37. Riminucci A, Dionigi C, Pernechele C, de Pasquale G, de Caro T, Ingo GM; Mezzadri F, Bock N, Solzi M, Padeletti G, Sandri M, Tampieri A, Dediu VA. Magnetic and Morphological Properties of Ferrofluid-Impregnated Hydroxyapatite/Collagen Scaffolds. Sci Adv Mater 204;6:2679-2687.
38. Rezakhaniha R, Agianniotis A, Schrauwen JT, Griffa A, Sage D, Bouten CV et al. Experimental investigation of collagen waviness and orientation in the arterial adventitia using confocal laser scanning microscopy. Biomech Model Mechanobiol 2002;11:461-73.
39. Rodriguez-Florez N, Oyen ML, Shefelbine SJ. Insight into differences in nanoindentation properties of bone. J Mech Behav Biomed Mater 2013;18:90-9.
40. Bianchi M, Boi M, Sartori M, Giavaresi G, Lopomo N, Fini M et al. Nanomechanical Mapping Of Bone Tissue Regenerated By Magnetic Scaffolds. J Mater Sci Mater Med 2015;26:35-43.

41. Oliver WC, Parr GM. Measurement of hardness and elastic modulus by instrumented indentation: advances in understanding and refinements to methodology J Mater Res 2004;19:3-20.
42. Bianchi M, Russo A, Lopomo N, Boi M, Maltarello MC, Sprio S et al. Pulsed Plasma Deposition of zirconia thin films on UHMWPE: proof of concept of a novel approach for joint prosthetic implants. J Mater Chem B 2013;1:310-8.
43. Ishimoto T, Nakano T, Yamamoto M, Tabata Y. Biomechanical evaluation of regenerating long bone by nanoindentation. J Mater Sci Mater Med 2011;22:969-76.
44. Bala Y, Depalle B, Douillard T, Meille S, Clément P, Follet H et al. Respective roles of organic and mineral components of human cortical bone matrix in micromechanical behavior: an instrumented indentation study. J Mech Biomed Mater 2011;4:1473-82.
45. Torbet J, Ronziere M. Magnetic alignment of collagen during self-assembly. Biochem J 1984;219:1057-9.
46. Ueno S, Iwasaka M, Eguchi H, Kitajiama T. Dynamic behavior of gas-flow in gradient magnetic-fields. IEEE Trans Mag 1993;29:3264-6.
47. Kotani H, Iwasaka M, Ueno S. Magnetic orientation of collagen and bone mixture. J Appl Phys 2000;87:6191-3.
48. Mannix JR, Kumar S, Cassiola F, Montoya-Zavala M, Feinstein E, Prentiss M et al. Nanomagnetic actuation of receptor-mediated signal transduction. Nat Nanotech 2008;3:36-40.

Figure captions

Figure 1

Schematic summary of the *in vivo* experiment planned to investigate the effect of combination of permanent magnets and magnetized biomaterials on the regeneration of bone tissue (top). 4 different groups (MAG A, MAG B, MAG C and MAG D) with permanent magnets were considered. Only MAG A and MAG B groups contained magnetized scaffolds (Magnetic Groups). As control groups, permanent magnet only (MAG C) or non-magnetized scaffolds (MAG D) were selected. Scaffolds and permanent magnets were implanted in the femoral condyle of rabbits and retrieved after 12 weeks from surgery. SEM images of MAG A (scale bar is 200 μm), MAG B and MAG D (scale bar is 400 μm) evidencing a similar porous 3D architecture (bottom).

Figure 2

Representative radiological (a) and optical (b, MAG C, scale bar is 3 mm) images of retrieved implanted condyles, from which the preservation of a correct positioning of the NdFeB permanent magnet at 12 weeks from surgery can be observed. In c) a detail of the intimate contact between newly-formed bone and the surface of the permanent magnet (c, MAG C, scale bar is 300 μm). In d) the image of a not implanted condyle is shown in order to show normal bone growth in the investigated region (scale bar is 3 mm). In the radiological image (a), the permanent magnet appears white, whereas in the histological images (b, c) it is black. In a-c) bone tissue appears green/light blue while bone marrow appears white/transparent.

Figure 3

Details of histological sections of the four investigated groups showing bone growth in the implantation area after 12 weeks from implantation. Large (a, c; scale bar: 1 mm) and detailed (b, d; scale bar: 500 μm) of magnetic groups MAG A (a, b) and MAG B (c, d). Large (e, g; scale bar: 2 mm) and detailed (f, h; scale bar: 200 μm) of control groups MAG C (e, f) and MAG D (g, h). The permanent magnet is black; mature regenerated bone as well as native bone is stained in green, whereas woven bone visible in c) and d) is stained in light blue; brownish material is the residual magnetized scaffold collagen fibers. Red lines and arrows help the visualization of the regeneration area. Out with this region, native bone is present.

Figure 4

BSE images (a, b) and EDX maps (c, d) of the same site are shown in order to localize the elemental atomic distribution of iron in the area of bone regeneration. Red stars and parallel white arrows in a) and b) indicate the presence of normal osteocyte lacunae and the direction of the magnetic field lines, respectively. In c) and d) iron is marked in red, calcium in green. Scale bar is 50 μm.

Figure 5

Histomorphometric analysis data. A) newly-formed bone results of MAG A, MAG B, MAG C and MAG D at 12 weeks after surgery. B) Scaffold material results of MAG-A and MAG-B at 12 weeks after surgery. Mean ± SD, n=6, *$p < 0.05$.

Figure 6

Results of the trabecular orientation analysis. Percentage of trabecular structures of MAG A, MAG B, MAG C and MAG D oriented inside the defect in the + (-) 90° to + (-) 80° and -10° to +10° ranges. Mean ± SD, n=3, *$p < 0.05$.

Figure 7

BSE-EDX analysis performed on new bone trabeculae in order to determine the presence of iron nanoparticles within novel bone tissue at 12 weeks from surgery. Large view BSE image (a, scale bar is 100 μm) in which the red lines help the visualization of the darker regions exhibiting more fresh bone (less mineralized) compared to the more mature bone tissue which appears brighter (more mineralized). The EDX analysis was performed on brighter spots present both in the less mature (darker, b) and more mature (brighter, d) regions of bone tissue. In the less mineralized regions of bone tissue it was possible to detect some Fe particles (c). In contrast more mineralized tissue generally showed the absence of iron (e). In b) and d) scale bar is 3 μm.

Figure 8

Regeneration pathway driven by magnetic forces comparing results seen at 4 (a, c, e)[32] and 12 (b, d, f) weeks for magnetic and control groups. Sketch of bone regeneration pattern (a and b); optical images of retrieved bone sections for magnetic (c, and d; scale bar is 100 μm) and control scaffold, (e, and f; scale bar is 400 μm). Optical images of retrieved bone sections indicated a regular bone regeneration pattern, with thick trabeculae orthogonally oriented with respect to magnetic field lines at 12 weeks from surgery (d). In absence of magnetic scaffold or when using a non-magnetic scaffold, this peculiar process does not occur (e, f). In c-f) bone tissue appears green/light blue, the residual scaffold material (magnetized collagen fibers) is brownish, the permanent magnet is black and the bone marrow (infiltrated by PMMA) appears white.

Table 1

Nanoindentation analysis data (E_r and H_c for new and native bone and mechanical gap %) for the four investigated groups. [a] $p < 0.05$ with respect to E or H of new bone.

Figure 1


Magnetic Scaffold
(4 x 4 mm)
1.2 T Cylindicar
NdFeB magnet
with titanium coat
(8 x 2 mm)
Magnetic Groups
Control Groups
MAG A
Co-nucleation of biomimetic HA and MNPs on collagen fibres + NdFeB magnet
MAG B
Infiltration of biomimetic HA/collagen scaffold with MNPs ferrofluid solution + NdFeB magnet
MAG C
NdFeB magnet only
MAG D
Biomimetic HA/collagen + NdFeB magnet
HA/collagen
HA nanocrystals
Fe3O4 MNPs ferro-fluid solution
MAG A
MAG B
MAG D

Figure 2

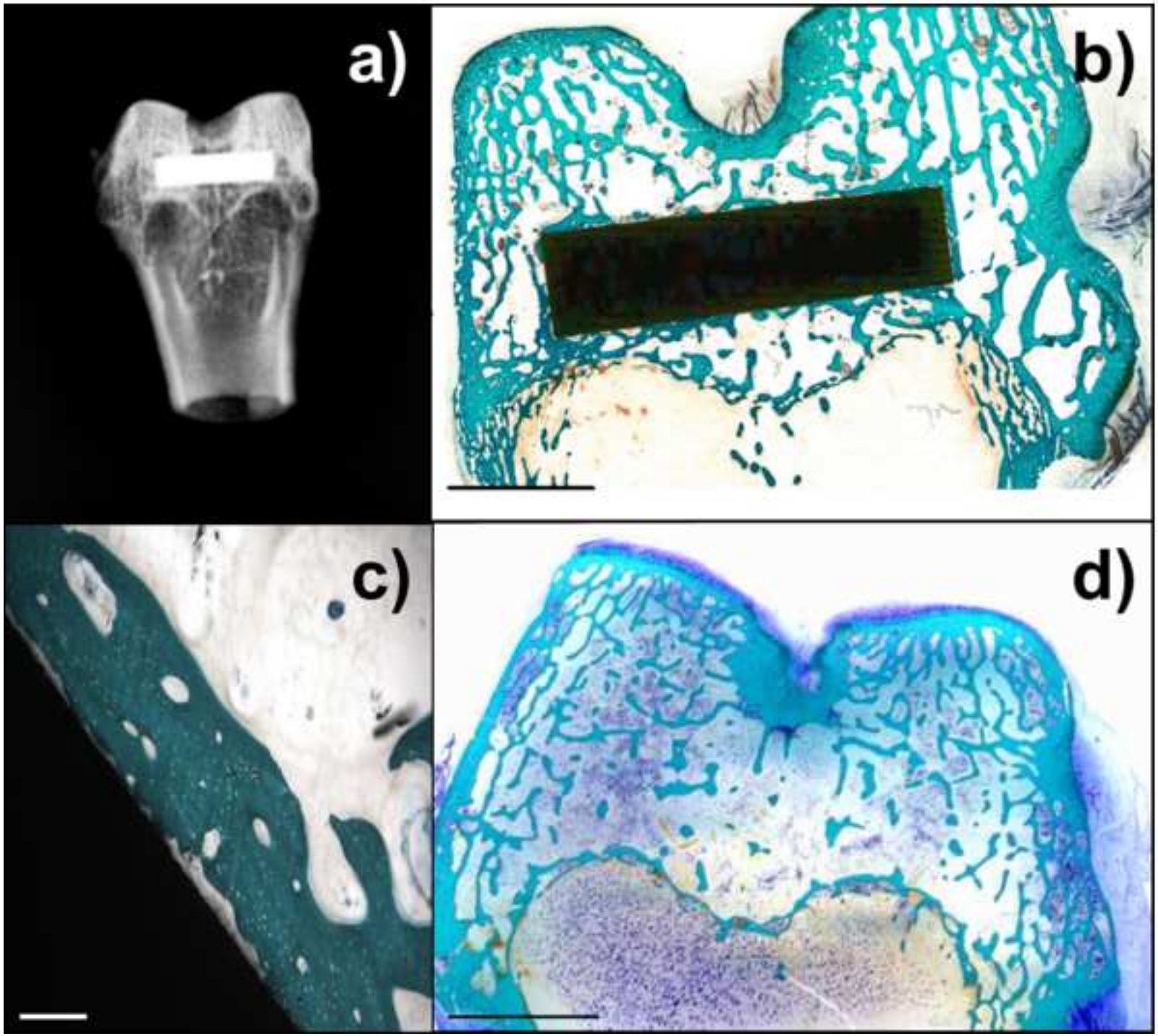

Figure 3

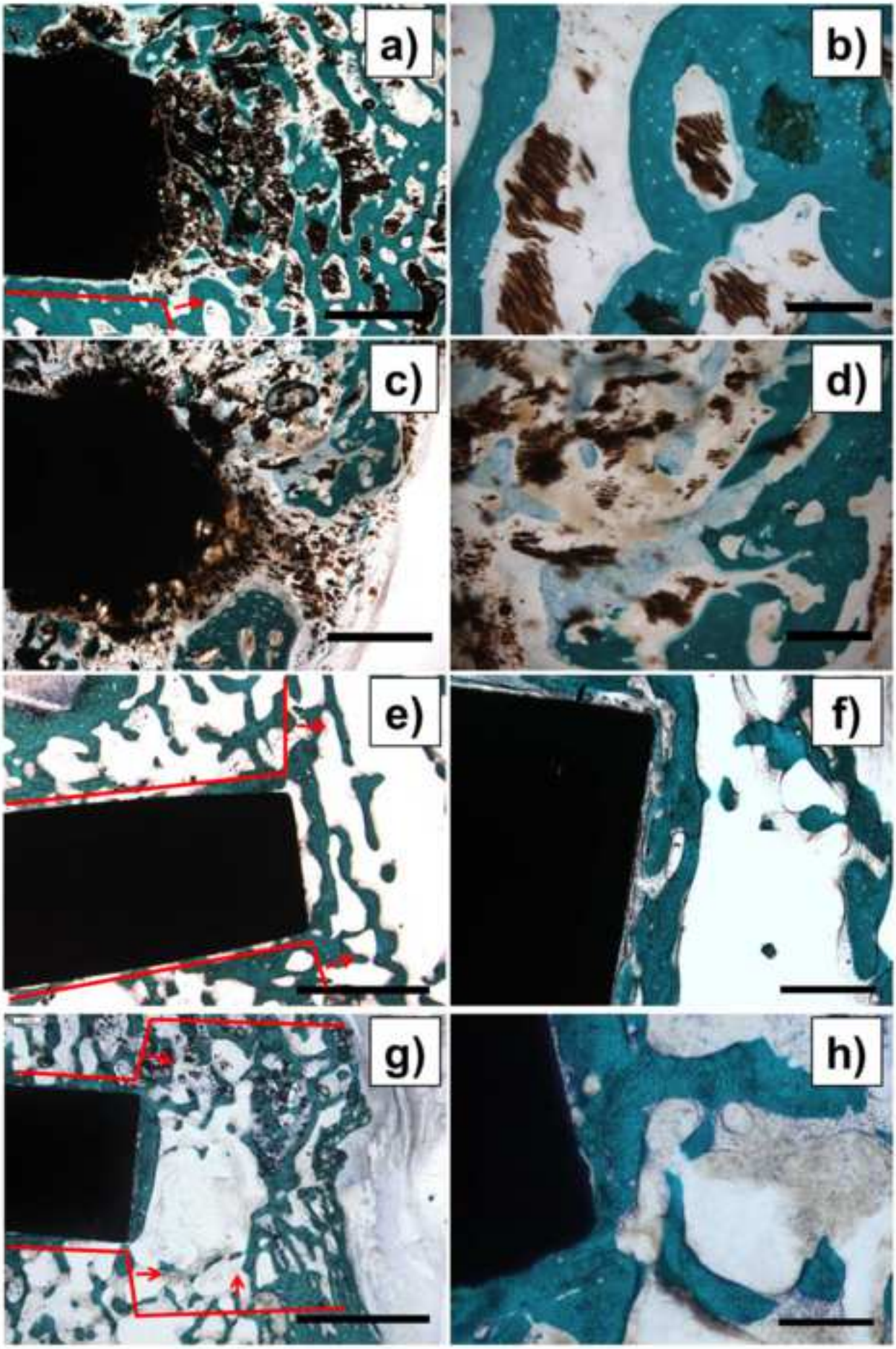

Figure 4

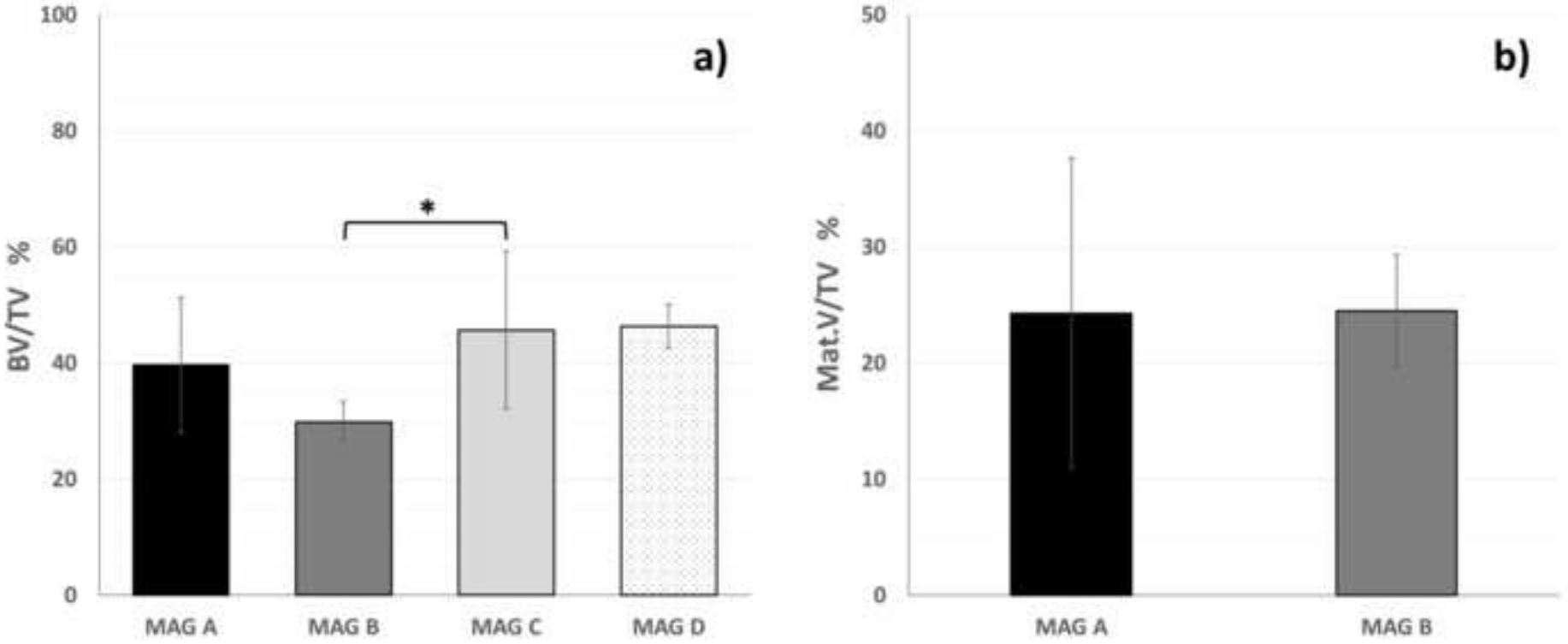
a)
BV/TV %
100
80
60
40
20
0
*
MAG A
MAG B
MAG C
MAG D
b)
Mat.V/TV %
50
40
30
20
10
0
MAG A
MAG B

Figure 5

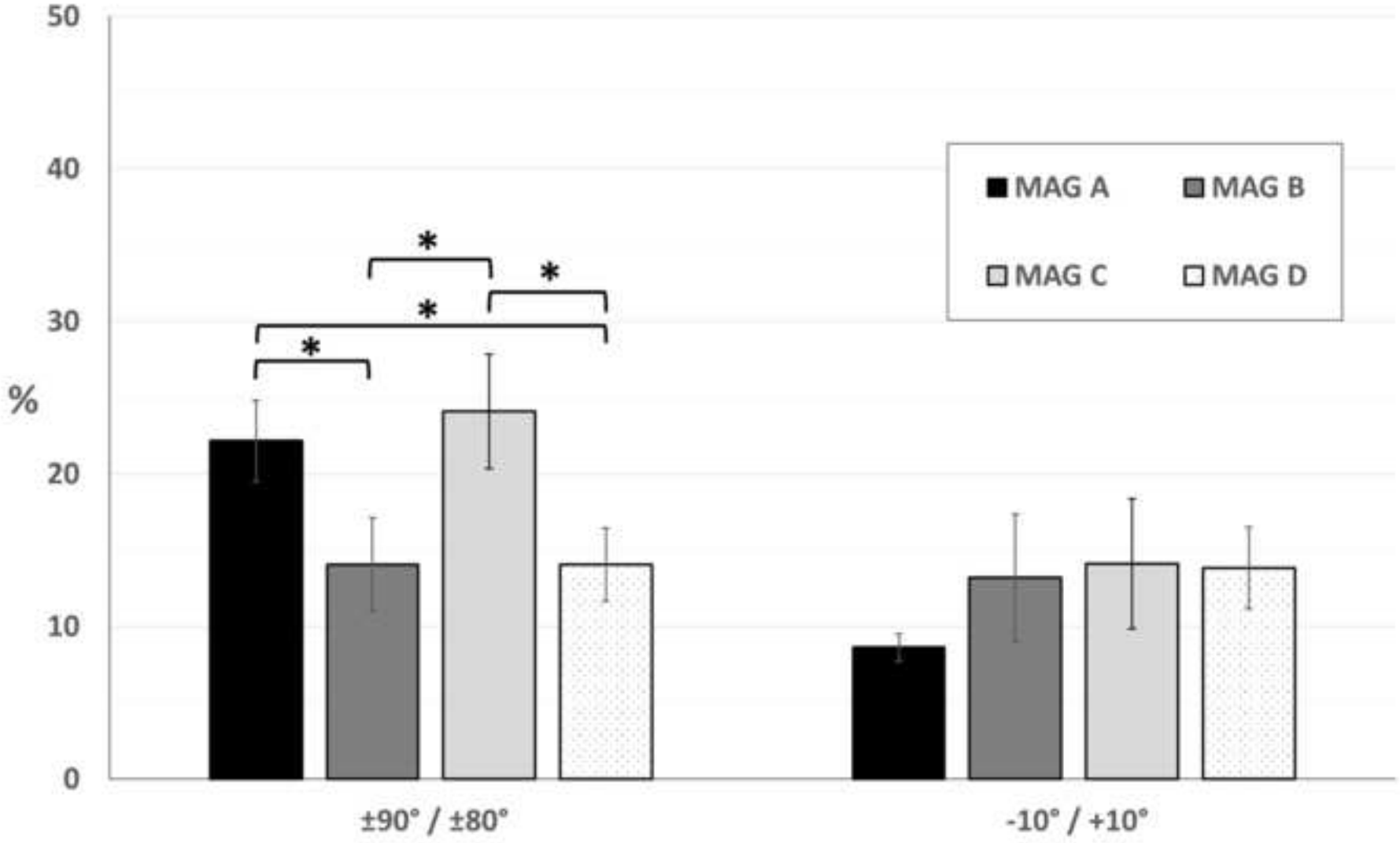

Figure 7

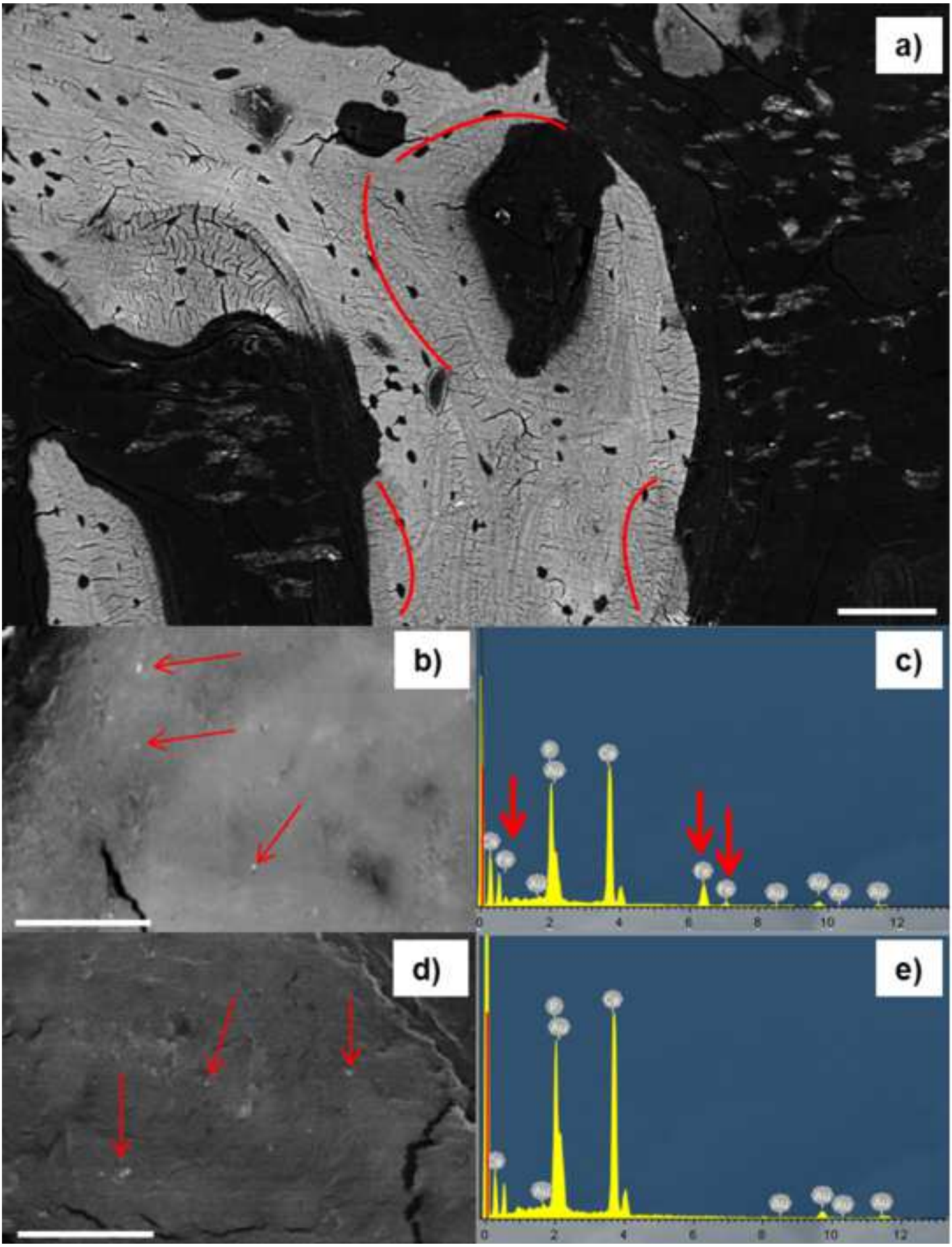

Figure 6

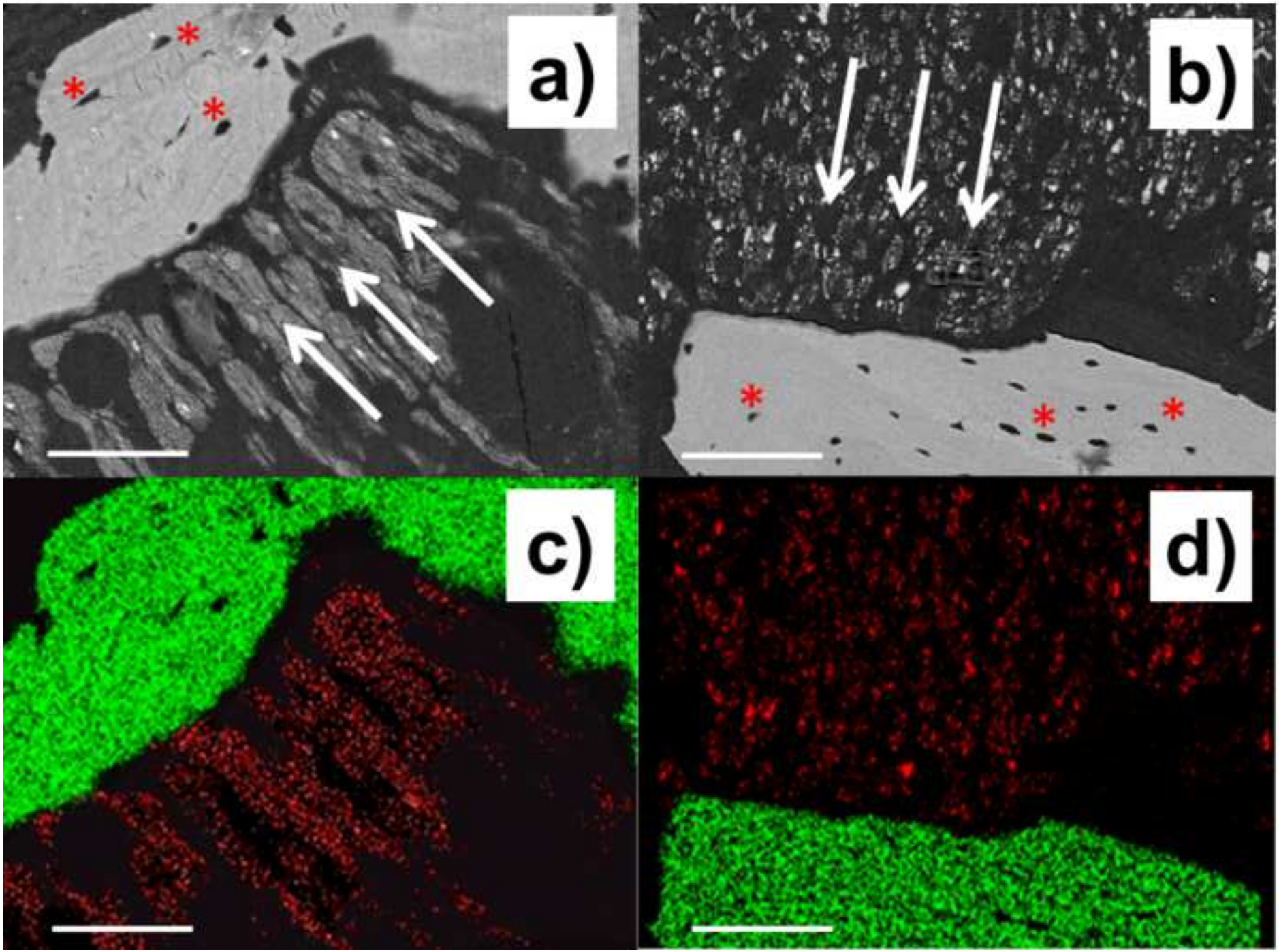

Figure 8

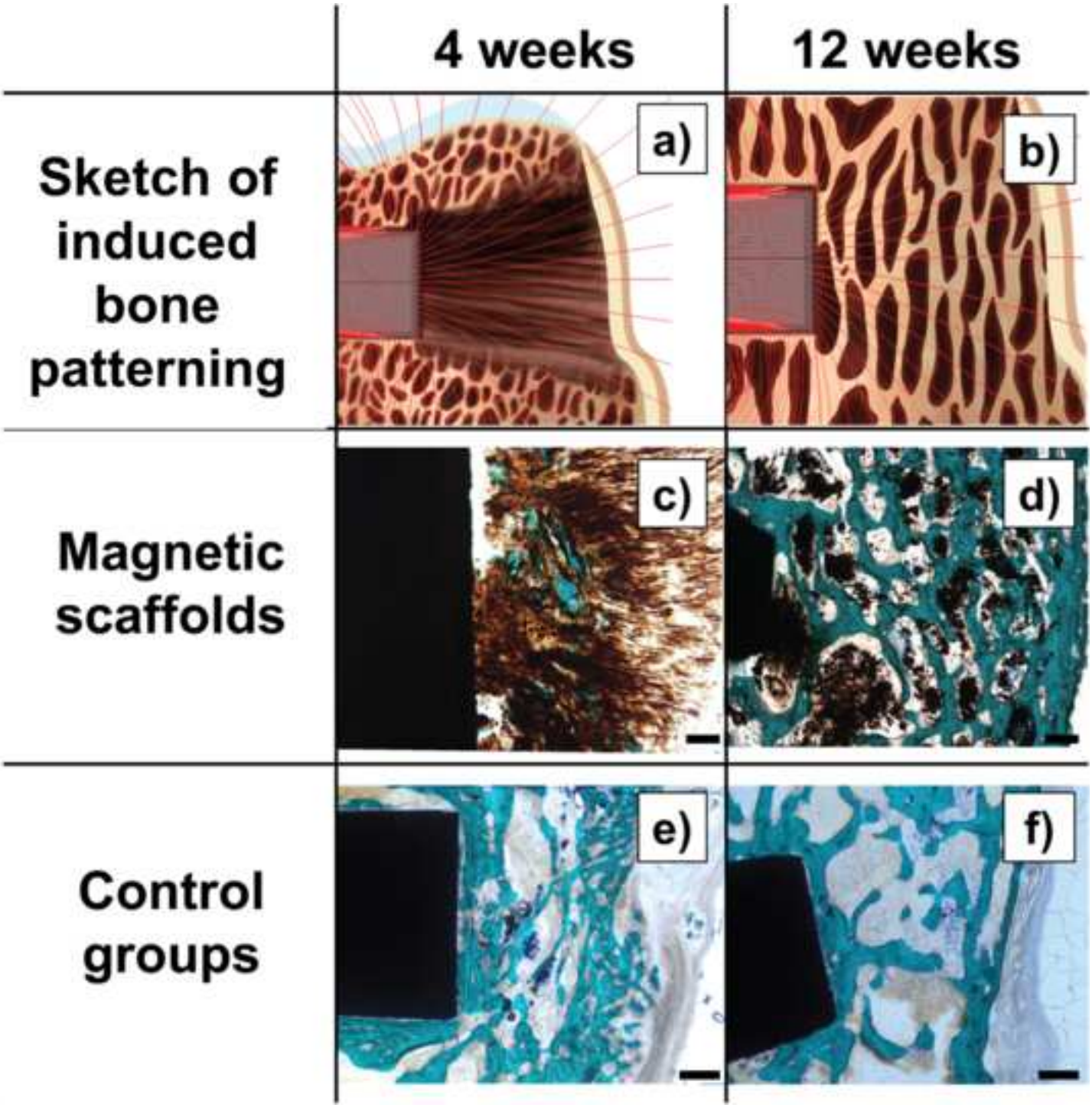
4 weeks
12 weeks
Sketch of induced bone patterning
Magnetic scaffolds
Control groups
a)
b)
c)
d)
e)
f)

Table

	MAG A	MAG B	MAG C	MAG D
Reduced Elastic Modulus				
$E_{new\ bone}$ (GPa)	12.8 ± 3.4	12.0 ± 3.1	12.2 ± 3.1	13.2 ± 2.1
$E_{native\ bone}$ (GPa)	13.6 ± 3.6[a]	14.0 ± 2.4[a]	15.1 ± 3.6[a]	15.7 ± 2.3[a]
Mechanical gap (%)	***6.1 ± 0.7***	***13.9 ± 9.3***	***19.2 ± 6.9***	***15.0 ± 0.6***
Contact Hardness				
$H_{new\ bone}$ (GPa)	531 ± 170	460 ± 164	450 ± 160	443 ± 108
$H_{native\ bone}$ (GPa)	520 ± 170	538 ± 189[a]	532 ± 162[a]	580 ± 120[a]
Mechanical gap (%)	***- (2.2 ± 1.3)***	***14.5 ± 7.9***	***15.4 ± 10.2***	***23.6 ± 2.2***